Stretchable Supercapacitors

Deutsche Ausgabe: DOI: 10.1002/ange.201603356
Internationale Ausgabe: DOI: 10.1002/anie.201603356

Highly Stretchable Supercapacitors Based on Aligned Carbon Nanotube/Molybdenum Disulfide Composites

*Tian Lv, Yao Yao, Ning Li, and Tao Chen**

Abstract: *Stretchable supercapacitors that can sustain their performance under unpredictable tensile force are important elements for practical applications of various portable and wearable electronics. However, the stretchability of most reported supercapacitors was often lower than 100 % because of the limitation of the electrodes used. Herein we developed all-solid-state supercapacitors with a stretchability as high as 240 % by using aligned carbon nanotube composites with compact structure as electrodes. By combined with pseudocapacitive molybdenum disulfide nanosheets, the newly developed supercapacitor showed a specific capacitance of 13.16 F cm^{-3}, and also showed excellent cycling retention (98 %) after 10000 charge–discharge cycles. This work also presents a general and effective approach in developing high-performance electrodes for flexible and stretchable electronics.*

With the rapid development of flexible electronics, stretchable energy storage devices, such as supercapacitors and lithium-ion batteries, that can bear unpredictable tensile forces have attracted increasing attention.[1–3] Compared with lithium-ion batteries, supercapacitors (also called electrochemical capacitors or ultracapacitors) have higher power densities, longer cycle lives, and easier fabricating processes, and are promising for use as power sources in portable electronics, electric or hybrid electric vehicles, especially for some fields requiring power with short-term acceleration and recovery.[4,5] Therefore, stretchable supercapacitors have been widely investigated, which can be easily realized by assembling two stretchable electrodes sandwiching a layer of gel electrolyte used as separator.[6–9] However, stretchabilities of most developed supercapacitors were lower than 100 %,[10,11] and the performance usually decreased shapely at high tensile strain. Furthermore, the specific capacitance of the developed stretchable supercapacitors was often lower than that of conventional devices. Both of the above mentioned problems can be ascribed to the limitation of the used electrodes. Therefore, highly stretchable supercapacitors with high specific capacitance may be achieved by optimizing the used electrodes and active materials.

Carbon nanotubes (CNTs) have been widely investigated as electrodes and/or active materials in supercapacitors because of their excellent electrical conductivity, mechanical properties, and large surface area.[12,13] Most of previous reported stretchable supercapacitors were developed by using CNTs materials because they can function as current collectors and active materials simultaneously.[14,15] However, the developed stretchable supercapacitors by using bare CNTs materials often showed relative low specific capacitance.[16–19] Therefore, highly pseudocapacitive materials (such as conducting polymers, metal oxides, and metal sulfides) were often combined with CNTs to enhance the performance of CNTs-based supercapacitors.[20–23] As a representative two-dimensional nanomaterial, the molybdenum disulfide (MoS_2) nanosheet, which is composed of one Mo atomic layer sandwiched between two S layers by covalent bonding, has attracted increasing attention in the field of energy storage, owing to its unique structure, excellent physical and chemical properties. Particularly, MoS_2 nanosheets not only showed high double-layer charge storage derived from its large surface area, but also can delivery excellent pseudocapacitance because of the Mo ions in the MoS_2 nanosheets have oxidation states ranging from $+2$ to $+6$, which enable them to be used as high-performance electrode materials in supercapacitors.[24–26] However, the relative low electrical conductivity of MoS_2 greatly limited the specific capacitance of the developed MoS_2-based supercapacitors. Therefore, it could be expected that stretchable supercapacitors with high-performance may be obtained by using aligned CNT/MoS_2 composites as the electrodes.

Herein, we designed a highly stretchable all-solid-state supercapacitor based on aligned CNTs electrodes, which not only can facilitate transport of charges through the electrode materials, but also can provide the devices with high stretchability. To start with, aligned CNT array was vertically grown on a silicon wafer coated with an iron catalyst by chemical vapor deposition approach. The CNT array was then pressed against an elastic polymer film (polydimethylsiloxane, PDMS), resulting in horizontally aligned CNTs attached on the surface of the PDMS substrate (CNTs/PDMS). Then, aligned CNT/MoS_2 hybrid was fabricated by directly drop-coating MoS_2 solution onto the CNTs film on the PDMS substrate. Flexible and stretchable supercapacitors were developed by using the CNT/MoS_2 hybrids as both of current collector and electrodes, sandwiched with gel electrolyte (aqueous solution of polyvinyl alcohol and phosphoric acid) in between (Figure 1). The newly developed all-solid-state supercapacitors showed a specific capacitance of 13.16 F cm^{-3}, which can be stretched by 240 % without obvious decay in electrochemical performance, much higher than that of most reported stretchable supercapacitors.

[*] Dr. T. Lv, Y. Yao, N. Li, Prof. T. Chen
Department of Chemistry, Institution of Advanced Study & Shanghai Key Lab of Chemical Assessment and Substainability
Tongji University
Shanghai 200092 (P.R. China)
E-mail: tchen@tongji.edu.cn

Supporting information for this article can be found under: http://dx.doi.org/10.1002/anie.201603356.

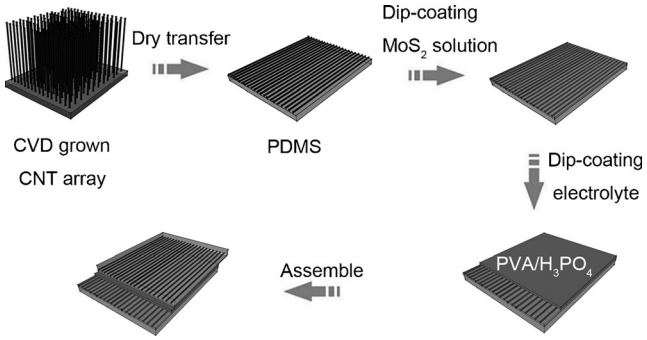

Figure 1. Schematic of fabrication process for the flexible and stretchable supercapacitor.

The aligned CNT array was synthesized through a chemical vapor deposition method described elsewhere.[27,28] In brief, the vertically aligned CNT array was grown on a silicon wafer pre-coated with Fe (1.2 nm)/Al_2O_3 (3 nm) under a mixture of argon and hydrogen as the carrier gas and ethylene as the carbon source at 760 °C. The as-grown CNT array showed a height of 240 μm and a highly aligned structure, which can be clearly observed from SEM images shown as Figure S1 of the Supporting Information. From TEM (transmission electron microscope) images (Figure S2), it can be seen that CNTs showed a multi-walled structure and uniform outer diameter of 11 nm. The vertically aligned CNT array was directly transferred onto an elastic substrate by pressing the preformed PDMS film on the top of CNT array using a glass rod, after being peeled off them from the silicon wafer, resulting horizontally aligned compact CNT film attached on the PDMS substrate. Figure 2 a,b presented the SEM image of as-transferred CNTs on PDMS substrate before and after solvent treatment, which clearly showed that CNTs highly aligned with each other along the direction of pressing force (Figure 2 b). The obtained horizontal CNT film showed a thickness of 8 μm (Figure S3), much thinner than that of as-grown vertically three-dimensional CNT array. The horizontal array is more suitable to be used as stretchable electrodes for stretchable electronics because slippage of CNTs position in the aligned films has a limited effect on the electrical property of the whole electrode during stretching process.

To prepared aligned CNT/MoS_2 composite films, MoS_2 nanosheets were synthesized by a typical hydrothermal method,[29] which was described in details in the experimental section in the Supporting Information. Then, aligned CNT/MoS_2 composite films were fabricated by directly dropping MoS_2 solution onto the horizontally aligned CNT film attached to the PDMS substrate. The MoS_2 content can be easily controlled by varying the dropping amount. Figure 2 c shows the SEM image of as-prepared MoS_2 nanosheets, which exhibited a flowerlike structure because of aggregation of the nanosheets. The MoS_2 nanosheets were characterized by TEM (Figure 2 d), which showed a two-dimensional structure and a typical polycrystalline structure (inset of Figure 2 d). From the high-magnification TEM image (Figure S4), the interlayer spacing of 0.62 nm and interplanar spacing of 0.27 nm can be observed, which can be ascribed to the (002) and (100) directions of hexagonal MoS_2, respectively. Figure 2 e,f show TEM images of CNT/MoS_2 composite, in which CNTs and MoS_2 nanosheets can be clearly observed.

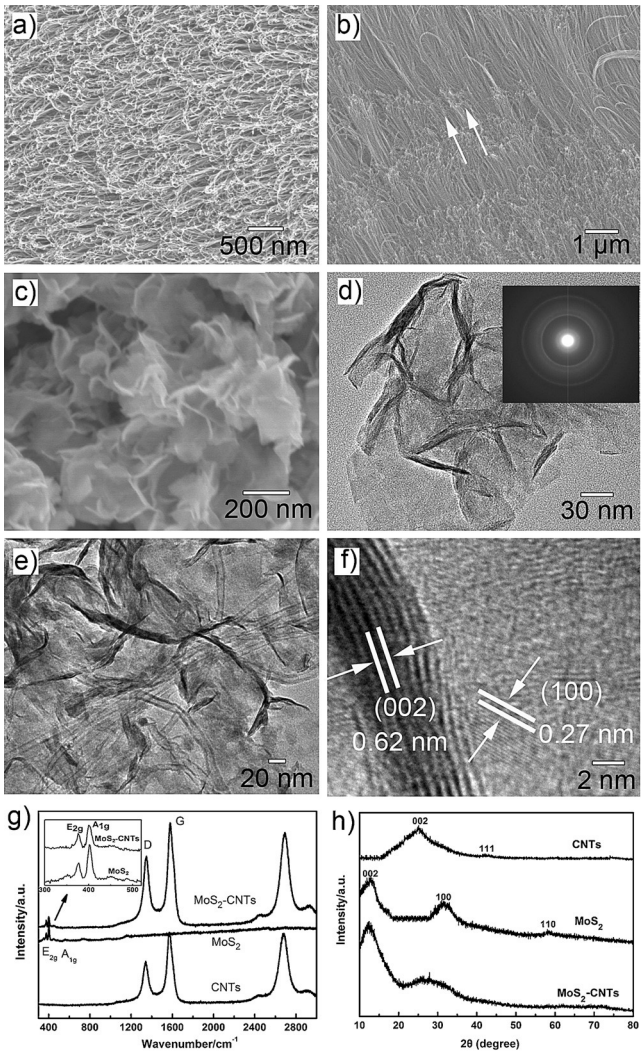

Figure 2. Morphology and structure of CNTs, MoS_2, and CNTs/MoS_2 composite with 5 wt% of MoS_2. a),b) The top-view SEM images of as-transferred CNTs on PDMS substrate before (a) and after (b) solvent treatment. The white arrows indicate the direction of pressing force and the aligned direction of CNTs. c) SEM image of as-synthesized MoS_2. d) TEM image of MoS_2 nanosheets. Inset: electron diffraction pattern. e),f) TEM images of the CNTs/MoS_2 composite after dispersed in dimethylformamide, at different magnifications. g) Raman spectra of CNTs, MoS_2, and CNTs/MoS_2. h) XRD patterns of the CNTs, MoS_2, and CNTs/MoS_2.

In CNT/MoS_2 composite film, the CNTs maintained their high alignment and compact structure (see Figure S5), which can provide more efficient charge transport through the electrode for supercapacitor applications. From Figure S5, it can also be seen that as the content of MoS_2 increased, more MoS_2 nanosheets aggregated together on the surface of aligned CNT films. Figure 2 g shows the Raman spectra of bare CNT film, as-prepared MoS_2, and CNT/MoS_2 composite film by using an excitation wavelength of 514 nm in ambient air. For bare CNT film, a D-band peak at 1352 cm^{-1} and a G-band peak at 1585 cm^{-1} can be observed, and the relative low

intensity ratio (ca. 0.6) between the D-band peak and G-band peak indicated that CNTs were very clean with high quality. For pure MoS_2, two peaks at 382 and 406 cm^{-1} can be ascribed to the E_{1g} and A_{1g} modes of hexagonal MoS_2 crystal, which involved the in-layer displacement of Mo and S atoms and the out-of-layer symmetric displacements of S atoms along the *c* axis, respectively. By measured the Raman spectrum within a certain area of CNT/MoS_2 composite without MoS_2 aggregations, both Raman shift derived from CNTs and MoS_2 can be seen, while both E_{1g} and A_{1g} band peaks of MoS_2 had a red-shift, which indicated that there was interaction between CNTs and MoS_2 in the CNT/MoS_2 composite.[30] From XRD patterns shown in Figure 2h, a peak at $2\theta = 26.2°$ for CNTs/MoS_2 composite can be attributed to the overlap between the (002) plane of CNTs (JCPDS card No. 15-1621) and the (100) crystal plane of hexagonal MoS_2 (JCPDS card No. 37-1492), which once again indicates that the CNTs and MoS_2 combine well and there is interaction between them.

Based on the aligned CNTs and CNT/MoS_2 composites, flexible and stretchable all-solid-state supercapacitors with high-performance have been developed by using an aqueous solution of polyvinyl alcohol (PVA) and phosphoric acid (H_3PO_4) as the gel electrolyte and separator (shown in Figure 1). Electrochemical properties of the obtained all-solid-state supercapacitors have been investigated by cyclic voltammograms (CV), galvanostatic charge-discharge (GDC) and electrochemical impedance spectroscopy (EIS). As shown in Figure 3a, all CV curves of supercapacitors based on CNTs composites with different MoS_2 contents showed typically rectangular shapes, indicating an ideal electrical double-layer behavior. Specially, CV curves of supercapacitor retained rectangular shapes as the scan rate increasing from 0.05 to 1.0 $V s^{-1}$ (Figure S6), indicating their excellent rate performance. GDC curves (shown in Figure 3b) of all the supercapacitors using CNTs composites containing different MoS_2 contents exhibited nearly triangular shape, exhibited good capacitive behavior. According to GDC curves, volumetric capacitances of supercapacitors can be calculated by using the equation of $C_V = I\Delta t/V\Delta V$, where I is the discharge current, V is the total volume of the active electrodes in supercapacitor, Δt is the discharging time, and ΔV is the voltage window. The supercapacitor fabricated by using CNTs composite containing 6.5 wt% of MoS_2 exhibited the highest specific capacitance of 13.16 $F cm^{-3}$ (corresponding to a gravimetric capacitance of 10.67 $F g^{-1}$), which also showed good excellent rate performance as its capacitance only decreased 17% with the charge-discharge current increased from 0.1 to 0.6 mA (Figure 3c,d). Figure 3e showed Ragone plots of CNT/MoS_2-based supercapacitors based on CNT composites with varying amount of MoS_2 (0, 5.0, 6.5, and 7.9 wt%), in which the energy density (E) and power density (P) were calculated according to the following equations, $E\ (Wh cm^{-3}) = 0.5 C_V V^2 * 1000/3600$ and $P\ (W cm^{-3}) = 3600\ E/t$, where t is the discharge time. The supercapacitor fabricated by using CNT/MoS_2 composite with 6.5 wt% of MoS_2 exhibited highest power density (0.46 $W cm^{-3}$) and energy densities (1.05 $mWh cm^{-3}$), which was much higher than that of other flexible supercapacitors reported previously.[31,32] The limitation of the PVA/H_3PO_4 electrolyte-based supercapacitors are their low output voltage (typically 0.8 V), which can be overcome by connected several devices in series. For instance, the output voltage can be tuned to 3.2 V (Figure S7a and S7b) by connected four supercapacitors in series, which

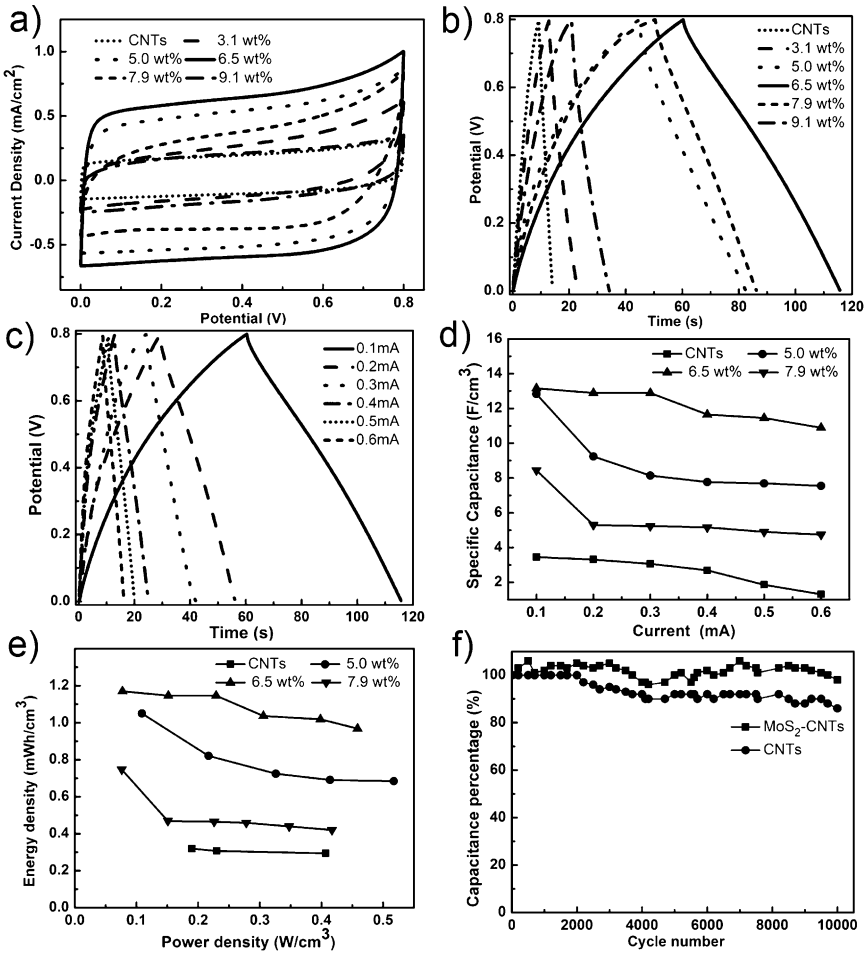

Figure 3. Electrochemical performance of supercapacitors based on CNT/MoS_2 composites with varying contents of MoS_2. a) CV curves of CNT/MoS_2-based supercapacitors at the scan rate of 0.1 $V s^{-1}$. b) GDC curves of supercapacitors at charge-discharge current of 0.1 mA. c) GDC curves of supercapacitor using CNT/MoS_2 composite with 6.5 wt% of MoS_2. d) Dependence of specific capacitances of supercapacitors on discharge currents. e) Ragone plots of MoS_2-CNTs-based supercapacitors with varying amount of MoS_2 (0, 5.0, 6.5, and 7.9 wt%). f) Cyclic performance of supercapacitors based on bare CNTs films and CNT/MoS_2 composite with 6.5 wt% of MoS_2 at a charge–discharge current of 0.5 mA.

was powerful enough to light up a light-emitting diode (LED) when fully charged (Figure S7c).

As a powerful tool, EIS has often been used to understand the electrochemical behaviors that occurred in the bulk electrode materials and/or at the interface between electrode and electrolyte in supercapacitors. Figure S8 showed the Nyquist plots of supercapacitors based on different CNT/MoS_2 composite electrodes. Series resistances (R_S) of supercapacitors can be obtained from the high frequency of Nyquist plots, which generated from the internal resistance of electrodes and Ohmic resistance of electrolyte. As the contents of MoS_2 increased from 0 to 3.1, 5.0, and 6.5 wt% in CNT composite films, R_S increased from 9.32 to 17.73, 22.98, and 24.75 Ω, respectively. Then, the R_S increased to 45.31 Ω as the content of MoS_2 increased to 7.9 wt%, almost one time higher than that of CNT/MoS_2 composite with 6.5 wt% MoS_2, which was the reason why the specific capacitance of supercapacitor decreased when MoS_2 contents in composite films increased from 6.5 to 7.9 wt%. In the low frequency, the straight lines almost vertical to the real axis, indicating that all supercapacitors exhibited an excellent capacitive behavior. The cycling stabilities of supercapacitors were measured through a cyclic charge–discharge process at a certain current. It can be seen from Figure 3f, the supercapacitor based on aligned CNT composite with 6.5 wt% MoS_2 showed an excellent capacitance retention (98%), much higher than that of supercapacitor based on bare CNTs (86%), which can be ascribed to the effective interaction between the MoS_2 nanosheet and CNTs.

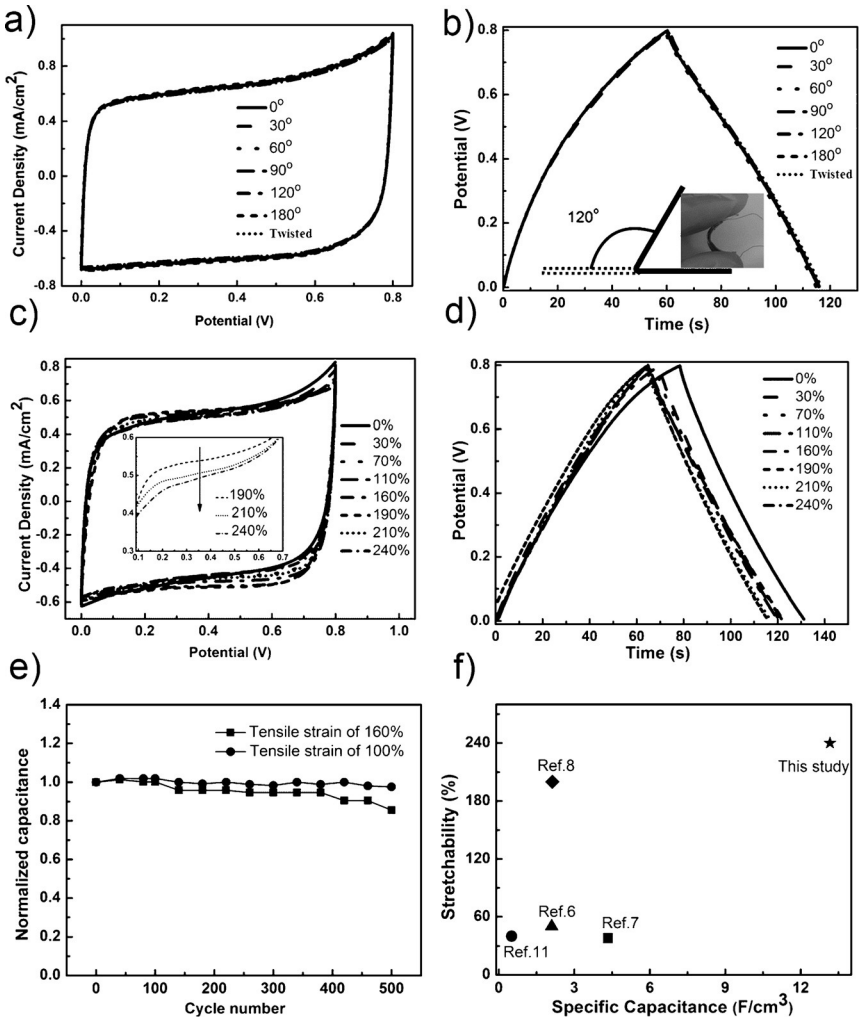

Figure 4. Flexible and stretchable properties of a supercapacitor fabricated by using CNT/MoS_2 composite films with 6.5 wt% of MoS_2 as electrodes. a) CV curves and b) Charge–discharge (at a current of 0.1 mA) curves of supercapacitor under different bending and twisted states. Inset shows schematic and digital photograph of supercapacitor being bent with 120°. c) CV curves of supercapacitor under different degrees of stretching varying from 0% to 240% at the scan rate of 0.1 Vs^{-1}. d) GDC curves of supercapacitor under different degrees of stretching at a current of 0.1 mA. e) Normalized specific capacitance of CNTs/MoS_2-based supercapacitor as a function of stretching cycles. f) Stretchabilities versus specific capacitances of our supercapacitor with other reported stretchable supercapacitors based on the same electrolyte system of PVA/H_3PO_4.

The flexibility and stretchability of our newly developed all-solid-state supercapacitors have been characterized by comparing their electrochemical performance under different bending states and various tensile strains, respectively. As shown in Figure 4a,b, both CV and GDC curves of the supercapacitor were perfectly overlapped and the electrochemical performances of the device were maintained well under various bending conditions even at 180° and twisting, exhibited excellent flexibility. The all-solid-state supercapacitor maintained its electrochemical performance (Figure 4c,d) as it was stretched from 0 to 240% at a constant stretching speed of 3 mm per minute, and only several white points appeared because of large slippage of CNTs in the electrodes under such high tensile strain (Figure S9). From Figure S10, it can be found that the specific capacitance of the testing supercapacitor slightly increased as the tensile strain increased from 0 to 190%, and slightly decreased as the tensile strain increased from 190 to 240%, which can be attributed to the increase of series resistance caused by slippage of CNTs in the electrodes under a such high tensile strain (Figure S11a). The CNT/MoS_2 composite-based supercapacitors can remain 96% and 91% of their original specific capacitance after being stretched to the strains of 100% and 160% for 500 cycles (Figure 4e), respectively, indicating outstanding stability. The R_S maintained in range of 26.1 to 27.5 Ω during 100 to 500 stretching cycles (Figure S11b), only slightly higher than original value (21.2 Ω), which can be ascribed to the high stretchability of the compact CNT-based electrodes whose electrical resistance only increased 150% (from 25.6 to 69.1 Ω) after being stretched to 240% strain

(Figure S12). To our knowledge, the stretchability of our newly developed supercapacitor is higher than that of other reported stretchable supercapacitors with the similar planar structure and electrolyte system (PVA/H_3PO_4, Figure 4 f).[6–8,11] The ultrahigh stretchability of our supercapacitors can be attributed to the highly stretchable PDMS substrate and the compact aligned CNTs bonded together by polymer chains in the gel electrolyte. In the compact CNTs film on PDMS, slippage of CNTs can be clearly observed during stretching process (Figure S13), and continuous CNTs (Figure S13 c) always remained even in the crack area, providing the aligned CNT-based electrodes with excellent stretchability, especially by coated with polymers.

In summary, we have demonstrated an efficient approach to develop highly stretchable all-solid-state supercapacitors by using aligned CNT/MoS_2 composite with a highly compact structure as electrodes. The supercapacitor fabricated by using a CNT/MoS_2 composite with 6.5 wt % of MoS_2 showed a high specific capacitance of 13.16 F cm^{-3} at a current density of 0.1 mA, as well as high cycling stability after 10000 cycling charge–discharge process. The all-solid-state supercapacitors exhibited excellent flexibility, whose electrochemical performance was almost unchanged under different bending states and even twisting. Significantly, these supercapacitors showed excellent stretchability as high as 240 % without obvious performance decay, which is higher than most of reported devices based on similar electrode and electrolyte system. Therefore, the highly flexible and stretchable supercapacitors are very promising to be used as high-performance energy source for other electronics, especially for variously stretchable integrated energy systems.

Acknowledgements

We acknowledge the support from The National Natural Science Foundation of China (No. 51503152), Science & Technology Commission of Shanghai Municipality (No. 14DZ2261100), The Program for Professor of Special Appointment (Eastern Scholar) at Shanghai Institutions of Higher Learning, and High-level Linghang Program of the Foundational Subjects in Tongji University.

Keywords: carbon nanotubes · molybdenum disulfide · stretchable · supercapacitors

How to cite: *Angew. Chem. Int. Ed.* **2016**, *55*, 9191 – 9195
Angew. Chem. **2016**, *128*, 9337 – 9341

[1] J. A. Rogers, Y. Huang, *Proc. Natl. Acad. Sci. USA* **2009**, *106*, 10875 – 10876.
[2] D.-H. Kim, N. Lu, R. Ma, Y.-S. Kim, R.-H. Kim, S. Wang, J. Wu, S. M. Won, H. Tao, A. Islam, K. J. Yu, T.-I. Kim, R. Chowdhury, M. Ying, L. Xu, M. Li, H.-J. Chung, H. Keum, M. McCormick, P. Liu, Y.-W. Zhang, F. G. Omenetto, Y. Huang, T. Coleman, J. A. Rogers, *Science* **2011**, *333*, 838 – 843.
[3] L. Yuan, X.-H. Lu, X. Xiao, T. Zhai, J. Dai, F. Zhang, B. Hu, X. Wang, L. Gong, J. Chen, C. Hu, Y. Tong, J. Zhou, Z. L. Wang, *ACS Nano* **2012**, *6*, 656 – 661.
[4] J. R. Miller, P. Simon, *Science* **2008**, *321*, 651 – 652.
[5] P. Simon, Y. Gogotsi, *Nat. Mater.* **2008**, *7*, 845 – 854.
[6] S. Y. Hong, J. Yoon, S. W. Jin, Y. Lim, S.-J. Lee, G. Zi, J. S. Ha, *ACS Nano* **2014**, *8*, 8844 – 8855.
[7] M. Yu, Y. Zhang, Y. Zeng, M.-S. Balogun, K. Mai, Z. Zhang, X. Lu, Y. Tong, *Adv. Mater.* **2014**, *26*, 4724 – 4729.
[8] Y. Meng, Y. Zhao, C. Hu, H. Cheng, Y. Hu, Z. Zhang, G. Shi, L. Qu, *Adv. Mater.* **2013**, *25*, 2326 – 2331.
[9] Y. Huang, M. Zhong, Y. Huang, M. Zhu, Z. Pei, Z. Wang, Q. Xue, X. Xie, C. Zhi, *Nat. Commun.* **2015**, *6*, 10310.
[10] N. Li, G. Yang, Y. Sun, H. Song, H. Cui, G. Yang, C. Wang, *Nano Lett.* **2015**, *15*, 3195 – 3203.
[11] Y. Sun, R. B. Sills, X. Hu, Z. W. Seh, X. Xiao, H. Xu, W. Luo, H. Jin, Y. Xin, T. Li, Z. Zhang, J. Zhou, W. Cai, Y. Huang, Y. Cui, *Nano Lett.* **2015**, *15*, 3899 – 3906.
[12] R. H. Baughman, A. A. Zakhidov, W. A. de Heer, *Science* **2002**, *297*, 787 – 792.
[13] M. Noked, S. Okashy, T. Zimrin, D. Aurbach, *Angew. Chem. Int. Ed.* **2012**, *51*, 1568 – 1571; *Angew. Chem.* **2012**, *124*, 1600 – 1603.
[14] N. Jha, P. Ramesh, E. Bekyarova, M. E. Itkis, R. C. Haddon, *Adv. Energy Mater.* **2012**, *2*, 438 – 444.
[15] T. Chen, H. Peng, M. Durstock, L. Dai, *Sci. Rep.* **2014**, *4*, 3612.
[16] A. E. Fischer, K. A. Pettigrew, D. R. Rolison, R. M. Stroud, J. W. Long, *Nano Lett.* **2007**, *7*, 281 – 286.
[17] S.-B. Ma, K.-W. Nam, W.-S. Yoon, X.-Q. Yang, K.-Y. Ahn, K.-H. Oh, K.-B. Kim, *J. Power Sources* **2008**, *178*, 483 – 489.
[18] S.-L. Chou, J.-Z. Wang, S.-Y. Chew, H.-K. Liu, S.-X. Dou, *Electrochem. Commun.* **2008**, *10*, 1724 – 1727.
[19] Z. Niu, H. Dong, B. Zhu, J. Li, H. Hng, W. Zhou, X. Chen, S. Xie, *Adv. Mater.* **2013**, *25*, 1058 – 1064.
[20] C. Meng, C. Liu, S. Fan, *Electrochem. Commun.* **2009**, *11*, 186 – 189.
[21] Z. Cai, L. Li, J. Ren, L. Qiu, H. Lin, H. Peng, *J. Mater. Chem. A* **2013**, *1*, 258 – 261.
[22] C. Choi, J. A. Lee, A. Y. Choi, Y. T. Kim, X. Lepró, M. D. Lima, R. H. Baughman, S. J. Kim, *Adv. Mater.* **2014**, *26*, 2059 – 2065.
[23] K. Wang, Q. Meng, Y. Zhang, Z. Wei, M. Miao, *Adv. Mater.* **2013**, *25*, 1494 – 1498.
[24] L. Cao, S. Yang, W. Gao, Z. Liu, Y. Gong, L. Ma, G. Shi, S. Lei, Y. Zhang, S. Zhang, R. Vajtai, P. M. Ajayan, *Small* **2013**, *9*, 2905 – 2910.
[25] E. G. d. S. Firmiano, A. C. Rabelo, C. J. Dalmaschio, A. N. Pinheiro, E. C. Pereira, W. H. Schreiner, E. R. Leite, *Adv. Energy Mater.* **2014**, *4*, 1301380.
[26] G. Sun, X. Zhang, R. Lin, J. Yang, H. Zhang, P. Chen, *Angew. Chem. Int. Ed.* **2015**, *54*, 4651 – 4656; *Angew. Chem.* **2015**, *127*, 4734 – 4739.
[27] M. Zhang, S. Fang, A. A. Zakhidov, S. B. Lee, A. E. Aliev, C. D. Williams, K. R. Atkinson, R. H. Baughman, *Science* **2005**, *309*, 1215 – 1219.
[28] H. Peng, *J. Am. Chem. Soc.* **2008**, *130*, 42 – 43.
[29] G. Ma, H. Peng, J. Mu, H. Huang, X. Zhou, Z. Lei, *J. Power Sources* **2013**, *229*, 72 – 78.
[30] W. Zhang, C.-P. Chuu, J.-K. Huang, C.-H. Chen, M.-L. Tsai, Y.-H. Chang, C.-T. Liang, Y.-Z. Chen, Y.-L. Chueh, J.-H. He, M.-Y. Chou, L.-J. Li, *Sci. Rep.* **2014**, *4*, 3826.
[31] X. Xiao, T. Li, P. Yang, Y. Gao, H. Jin, W. Ni, W. Zhan, X. Zhang, Y. Cao, J. Zhong, L. Gong, W.-C. Yen, W. Mai, J. Chen, K. Huo, Y.-L. Chueh, Z. L. Wang, J. Zhou, *ACS Nano* **2012**, *6*, 9200 – 9206.
[32] D. Yu, K. Goh, Q. Zhang, L. Wei, H. Wang, W. Jiang, Y. Chen, *Adv. Mater.* **2014**, *26*, 6790 – 6797.

Received: April 6, 2016
Revised: May 13, 2016
Published online: June 22, 2016

